Summer 2014

The effects of chronic neural implantation on localized vasculature

Andrew L. Ready
Purdue University

Graduate School ETD Form 9
(Revised 01/14)

PURDUE UNIVERSITY
GRADUATE SCHOOL
Thesis/Dissertation Acceptance

This is to certify that the thesis/dissertation prepared

By Andrew Ready

Entitled

The Effects of Chronic Neural Implantation on Localized Vasculature

For the degree of Master of Science in Biomedical Engineering

Is approved by the final examining committee:

Kevin Otto

Edward Bartlett

Sarah Calve

To the best of my knowledge and as understood by the student in the *Thesis/Dissertation Agreement. Publication Delay, and Certification/Disclaimer (Graduate School Form 32)*, this thesis/dissertation adheres to the provisions of Purdue University's "Policy on Integrity in Research" and the use of copyrighted material.

Approved by Major Professor(s): Kevin Otto

Approved by: George R. Wodicka 8/1/14

Head of the Department Graduate Program Date

THE EFFECTS OF CHRONIC NEURAL IMPLANTATION ON LOCALIZED VASCULATURE

A Thesis

Submitted to the Faculty

of

Purdue University

by

Andrew L. Ready

In Partial Fulfillment of the

Requirements for the Degree

of

Master of Science in Biomedical Engineering

August 2014

Purdue University

West Lafayette, Indiana

ACKNOWLEDGEMENTS

I'd like to thank Dr. Kevin Otto and Dr. Sarah Calve for their support during the course of my time here at Purdue, and for pushing me to refine and improve my techniques and research time and time again. I'd also like to thank everyone in the Purdue NPR for their suggestions and assistance in research, and for giving the moral and personal support. I am extremely grateful to Ashley Eidsmore and Roy Lycke for their guidance and assistance in developing the methodology to clean and quantify data, and for continuing to help even when times were rough. Thanks for keeping me sane.

TABLE OF CONTENTS

Page

LIST OF TABLES

LIST OF FIGURES

ABSTRACT

Ready, Andrew L. M.S.B.M.E., Purdue University, August 2014. The Effects of Chronic Neural Implantation on Localized Vasculature. Major Professor: Kevin Otto.

Prosthetic solutions currently available range from simple devices intended for aesthetics purposes to complex systems attempting to restore lost function and sensation; of these methods, none show more promise in restoration of normal function and life satisfaction than neural prosthetics. These devices directly interface with the nervous system in order to restore realistic function and feeling to the patient, potentially returning them to how their life once was. While in some cases patients requiring prosthetics can utilize peripheral nerves, those who suffer from injuries or disease which cause damage to the central nervous system can necessitate the usage of devices implanted directly into the brain or spinal cord. Research has shown that these implants lose efficacy over time due to the immunological reaction of the brain to injury, mirroring the foreign body response occurring in the rest of the body; these devices become encapsulated by scar tissue and local cells die or migrate over time. Outside of the response of cells like microglia and astrocytes to the injury, there is another factor influencing how the brain responds to injury: the vascular response. Previous experiments have shown the presence of visible vasospasms during and after implantation, as well as potential vasoconstriction in chronically implanted animals. As the vascular response can influence the survival of

nearby cells as well as portions of the immunological response, as evidenced by stroke, Reversible cerebral vasoconstriction syndrome (RVCS), and other disorders which occur due to vascular abnormalities, understanding how local vasculature responds to chronic implantation is an important step in developing methods to maintain function for chronically implanted devices.

In order to quantify this response, we implanted shank electrodes into 12 animals and then sacrificed them at separate time points that already have a well characterized immunological response. The brains extracted from these animals were then sliced in order to capture the implant intact and stained to allow for confocal imaging. These images were then cleaned and post-processed to extract information on the blood vessels present, allowing for the quantification of vascular segment diameter and length. Our resulting data shows that local vasodilation occurs almost immediately following the initial implantation, and is still occurring at 7 days afterward. Furthermore, our data suggests that there is a degree of systemic vasodilation, as over the course of 7 days we find an increase in the vascular diameter present in the opposite hemisphere where no injury has occurred.

CHAPTER 1. INTRODUCTION

1.1 Background

Prosthetics is a continuously advancing field, with advancements striving toward the restoration or replacement of lost function, feeling, and life satisfaction. In recent history, the field of prosthetics has advanced from simple wood and plastic replacements to computer controlled artificial knees and myoelectrically driven limb replacements (Ott, Serlin, & Mihm, 2002). The optimal prosthetic device should offer restoration to both lost function and sensation, allowing the patient to live as close to normal as they can. These devices, however, are not yet at a developmental level where they are on par with their undamaged counterparts. In time, those who suffer from injuries or disorders necessitating prosthetics may not suffer from any changes to their lives, or may even have improved capabilities in some way; however, there is still a long way to go and a lot of research and development to be done before this is a reality.

1.1.1 Prosthetics Market and Breakdown

There are many different situations where a prosthetic may be desired or needed by a patient including aesthetic replacements, replacements for damage brought on by disease (Pibarot & Dumesnil, 2009), and those necessary to compensate for injury are all potential reasons that a patient may receive a prosthetic (McGimpsey & Bradford, 2008).

Because of this, the field of prosthetics is quite large, containing craniofacial prostheses, neck prostheses, as well as upper and lower extremity prostheses. As an example of the prosthetic population, there are over 1.5 million amputees in the United States alone who utilize upper and lower limb prosthetic solutions, with this number growing by an estimated 185,000 each year (McGimpsey & Bradford, 2008). This group includes a large number of veterans and soldiers who have received injury during combat, but the majority of the cases that necessitate devices like this are actually due to diabetes and various vascular diseases (American Diabetes Association, 2005; McGimpsey & Bradford, 2008). Other examples of the prevalence of prosthetics include the fact that there are over 100,000 cochlear implants across the world, and the worldwide dental prosthetics market is estimated at over 5 billion in 2013 alone (Haynes & Labadie, 2000; McGimpsey & Bradford, 2008). Within each of these different market components, there are many different competitors using various strategies in order to solve the same type of issues: restoration of function or sensation.

1.1.2 Prosthetic Solutions

For those injuries or diseases which have a severe impact on life satisfaction or everyday living, researchers have developed a number of different solutions. In the case of limb replacement, whether due to injury or disease, some of the potential solutions to the question of function replacement and sensory restoration that have shown the greatest results include techniques such as Targeted Muscle Reinnervation (TMR) (T. a Kuiken, Dumanian, Lipschutz, Miller, & Stubblefield, 2004), myoelectrically driven prosthetics (Shannon, 1979), and joints with built-in microprocessors (Hafner, Willingham, Buell,

Allyn, & Smith, 2007). None of these solutions directly interface with the patient's neural system, but rather rely on indirect methods to receive signals for movement or to produce a sense of sensation. The most successful of these indirect solutions is the TMR procedure. In TMR, neurons that would normally cause movement in the missing area are reconnected to a muscle in the chest. The prosthetic then uses the myoelectric signals from this muscle to determine movement, and potentially uses a small motor to give a sense of haptic feedback (T. Kuiken, Miller, & Lipschutz, 2007).

While true neural prosthetics in the field of limb replacement are still under development and are commercially rare, devices which utilize the principles of neuroprosthetics are becoming more and more common. A prime example of a device which can be classified as a neuroprosthetic is a cochlear implant (Haynes & Labadie, 2000). These devices, intended for those who have some form of hearing impairment due to middle or inner ear damage, directly stimulate the auditory nerve located in the cochlea. While far from perfect, these devices offer hearing and speech comprehension to those who previously struggled with or were unable to hear. Another example of a technique utilizing a neuro-stimulating device is Deep Brain Stimulation (DBS) (Benabid, 2003), a procedure used in a number of cases which involves the installation of a brain pacemaker (Perlmutter & Mink, 2006a). This technique is commonly used for the treatment of Parkinson's disease, but is also approved for treating disorders like dystonia and obsessive compulsive disorder. While the exact method through which the device influences these disorders is not understood currently, regular electrical stimulation to regions of the brain such as the subthalamic nucleus and the globus pallidus interna positively influence the symptoms of the diseases and disorders this technique is approved to treat (Perlmutter & Mink, 2006b).

Unlike cochlear implants and the devices used in DBS which only interface with the central nervous system, limb prosthetics have two main locations where they directly can potentially interface with the nervous system: the central nervous system, including the brain and spinal cord, and the peripheral nervous system which includes those nerves in the rest of the body. Individuals who suffer from limb loss alone could potentially utilize either variety of neuroprosthetic, while patients who suffer from neurodegenerative disease or brain/spinal damage can likely only use a device of the Central Interface family. In these cases, the lost signal propagation from the brain makes it impossible to record neural signals in the peripheral nervous system.

1.1.3 Neural Stimulation and Recording

Neuroprosthetics rely on communicating directly with the patient's nervous system in order to send and receive information using neural communication. By recording neuronal signals intending to trigger movement and stimulating sensory nerves in response to tactile stimulation of the prosthetic, these devices aim to restore a semblance of normal function and sensitivity to the patient (McFarland & Wolpaw, 2011). The stimulating aspect allows the electrode to causes changes in the local field potential, which results in the influx of sodium into nearby neurons and the triggering of action potentials, which in turn can lead to sensation (Chang, 1951). Recording is accomplished through monitoring the field potential, which changes during neuronal firing and action potential propagation. The information recorded is processed in order to separate the spikes caused by neuronal firing from background data – the pattern behind the firing can then be processed in order to determine meanings, such as movement or muscle

activation. Aside from maintaining the implant, the decoding of neuronal firing into movements is one of the major hurdles faced by neuroprosthetic devices.

There are two main ways to accomplish both the stimulation and recording necessary for a prosthetic of this variety to function: penetrating neural implants and non-penetrating devices. While non-penetrating devices, such as those based on Electrocorticography (ECoG) or Electroencephalography (EEG) methods of brain stimulation and recording partially bypass the foreign body response and cause a smaller tissue reaction within the brain, they are currently not at a developmental stage where they can reliably stimulate or record with the same resolution as a penetrating electrode (Krames, Peckham, & Rezai, 2009). Because of this, penetrating implants are a popular choice for research and development in the field of neuroprosthetics; however, they often cause localized damage to cells and disrupt vasculature in the area near the implant. This disruption leads to the body's foreign body response, a reaction which introduces a number of complicating factors to the function of a neuroprosthetic (Lotfi, 2007; Polikov, Tresco, & Reichert, 2005).

1.2 Foreign Body Response

Following an injury, the body responds in order to return to homeostasis. This is accomplished via a complex response to injury known as the foreign body response (Kumar, Abbas, & Aster, 2003). For implants in both the brain and the periphery, this immune response reaction is split into two stages: the acute response responding to damage accrued during surgery and implantation, and the chronic response caused when the body is unable to clear the implant through phagocytosis (J. Anderson, 1988).

In the periphery, the immune response is characterized by the local release of signaling factors in response to injury, including cytokines and chemokines as well as histamine and other cellular signals. The release of these factors leads to clot formation, local vasodilation and a number of other responses including cellular recruitment and activation. The vasodilation, as well as the chemical signals present from cells responding to injury (including Tumor Necrosis Factor alpha and Interleukin Family 1), allows for the migration of leukocytes and other immune cells to migrate from the vasculature into nearby tissue, in a process known as extravasation (Ahmed, 2011a). These cells, as well as local macrophages, change phenotype during activation to facilitate the elimination of infectious elements, expel or encapsulate debris, and begin to repair damage to the region (J. Anderson, 1988). In the case of debris which cannot be cleared or are resistant to degradation, macrophages will fuse together and form foreign body giant cells, encapsulating the debris that caused the local tissue damage. This is considered a hallmark of chronic inflammation in response to foreign materials (J. M. Anderson, Rodriguez, & Chang, 2008).

The peripheral immune response is mirrored in the central nervous system (CNS), although the specifics are different. The CNS is an immune-privileged site, due to the blood brain barrier generated by astrocytes (Becher, Prat, & Antel, 2000). Astrocytes wrap around vasculature, creating tight end junctions which prevent extravasation of most cell types into the brain. Due to this, the brain has its own set of immune and support cells known as glial cells. For the tissue response, the relevant cells are microglia and astrocytes. The microglial cells have phagocytic properties like macrophages, while the astrocytes perform structural maintenance and help to keep the blood brain barrier

intact (Becher et al., 2000). After injury, and the resultant blood brain barrier disruption, immune cells from the periphery undergo extravasation into the brain; this, as well as the chemical signals released from local cellular damage, trigger the activation and migration of nearby microglia to the site. In acute cases, the microglia will phagocytose foreign material and cells, and the astrocytes will recreate the blood brain barrier with a minimal amount of scar tissue (Potter, Buck, Self, & Capadona, 2012). However, in the case of a sustained foreign body such as an implant, when microglia fail to phagocytose the implant they enter a state known as frustrated phagocytosis and form multi-nucleated cell bodies reminiscent of the foreign body giant cells produced by macrophages in the periphery (Lotfi, 2007; Polikov et al., 2005). The microglia in turn recruit additional astrocytes, causing them to activate and migrate to the injury site to form a glial sheath in a process known as astrogliosis (Landis, 1994; Turner et al., 1999). The sheath is composed of scar tissue and layers of living and dead cells surrounding the implant which eventually allows the brain to restore the blood brain barrier's integrity and return it to a state of immune-privilege (Turner et al., 1999).

1.3 Vascular Response to Injury

As discussed earlier, after an injury occurs vasculature has a characteristic response in the body and plays a major role in both acute and chronic inflammation. With an acute injury, arterioles undergo vasoconstriction followed quickly by capillary vasodilation (Newby, 2000). This leads to an increase in the amount of blood present in the region of injury as well as the leakage of plasma (edema) which is responsible for the symptoms indicative of inflammation including redness, swelling, heat, and pain (Ahmed, 2011a). This

reaction and the increase in blood cause a large influx of platelets, immune cells, and nutrients which are important for the reactive response (Ahmed, 2011b). Depending on the severity of the damage or if an irritant material cannot be easily cleared, the tissue can undergo a range of responses, such as a return to normal state, fibrosis, abscess formation, or chronic inflammation. Chronic inflammation, the most common response to the continued presence of an implant, results in the continued dilation of the local vasculature and the region remains swollen (Ahmed, 2011a). In this situation, cells previously helpful to the process of tissue repair become toxic rather than helpful. This potentially leads to tissue degradation and cell destruction (Morganti-Kossmann, Rancan, Stahel, & Kossmann, 2002).

1.3.1 Cerebral Vasculature

In order to discuss the effects of an implant in the brain and how the tissue will respond, it is important to discuss the brain's relationship with vasculature. The brain receives roughly 15-20% of the total cardiac output (750 mL/min). It distributes this blood at a rate of about 50 mL per 100 grams of tissue, which highlights the large amount of blood and oxygen needed for brain function(Cipolla, 2009). The brain is also extremely sensitive to the amount of blood perfusion it receives. An excess can lead to conditions such as edema while too little can lead to ischemia and potential cell death. In order to buffer and control the amount of blood in the brain and maintain healthy amounts of perfusion, the brain's vasculature has the ability to auto-regulate: by dilating and constricting local vasculature as necessary, the brain is able to compensate for most situations, including metabolic rate changes, blood oxygenation changes and changes in

posture (Attwell et al., 2010). This regulation in the brain is thought to be controlled by a number of feedback systems, including a metabolic control, a myogenic control, and a neurogenic control system (Paulson, Strandgaard, & Edvinsson, 1990). These three controls are hypothesized to modify the vascular diameter based on influences like local oxygen demand caused by cellular activation, blood pressure changes across the blood brain barrier, and direct neural stimulation (Paulson et al., 1990).

1.3.2 Cerebral Vasculature Disruption

After a traumatic brain injury (TBI), vasculature in the brain becomes less controlled. The auto regulatory abilities of the brain tend to be disrupted or completely abolished during the course of the injury (Janjua & Mayer, 2003).Without auto regulatory capabilities intact, the brain's vasculature is incapable of compensating for changes in such things as blood pressure or oxygen content, as seen in Figure 1. This figure shows the relationship between the mean arterial pressure (MAP) and the cerebral blood flow (CBF); in the normal curve, the CBF is buffered to 50 mL/min even as the arterial pressure changes, while in the case of the absent autoregulatory function (potentially caused by a TBI) the buffer is not present. This leads to a greater risk of ischemia and cell death (Paulson et al., 1990). In addition, as with the inflammatory response in the rest of the body, local damage will cause cells to release pro-inflammatory factors which will cause the dilation of nearby vessels. In the brain, this vasodilation as well as the local blood brain barrier disruption caused by the damage allows for the extravasation of leukocytes and other immune cells into the previously immune-privileged location. The presence of these cells in the brain can further exacerbate the inflammatory response,

leading to a more severe reaction and increasing the risk of chronic neuroinflammation and/or cell death (Zindler & Zipp, 2010).

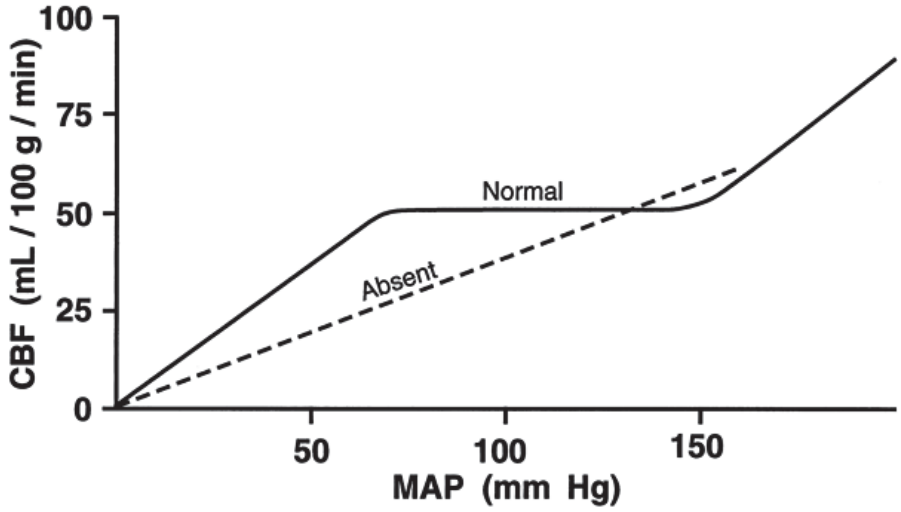

Figure 1: Cerebral auto-regulation curve in Normal and Traumatic Brain Injury
Adapted from Miller's Anesthesia 7th edition

1.4 Consequences of Chronic Cerebral Vascular Disruption

As discussed earlier, chronic inflammation due to the presence of foreign materials in the brain which cannot be cleared can lead to tissue damage and cell death caused by apoptosis and the release of toxins from previously helpful cells (Qin et al., 2007a). In addition, this can also lead to a state known as vasospasm, which is commonly caused when the chemical signaling agents released by platelets in response to vascular injury become contractive in nature rather than relaxing (Janjua & Mayer, 2003). In these cases, the spasming vasculature can lead to a dangerously low blood perfusion in regions of the brain, causing further cell death. Figure 2 showcases the degree of vasoconstriction which can occur This is especially prevalent after subarachnoid hemorrhages in the brain, but

can also appear due to a number of other factors as in the poorly understood Reversible Cerebral Vasculature Syndrome (RVCS) (Call et al., 1988; Sattar, Manousakis, & Jensen, 2010). Even in RVCS, which can have relatively mild symptoms in comparison to vasospasm that can occur following subarachnoid hemorrhage, sufferers report thunderclap headaches and a number of other neurological symptoms, the worst of which is actual stroke. In the case of vasospasm in response to subarachnoid hemorrhage, there is up to a 40-50% morbidity rate.

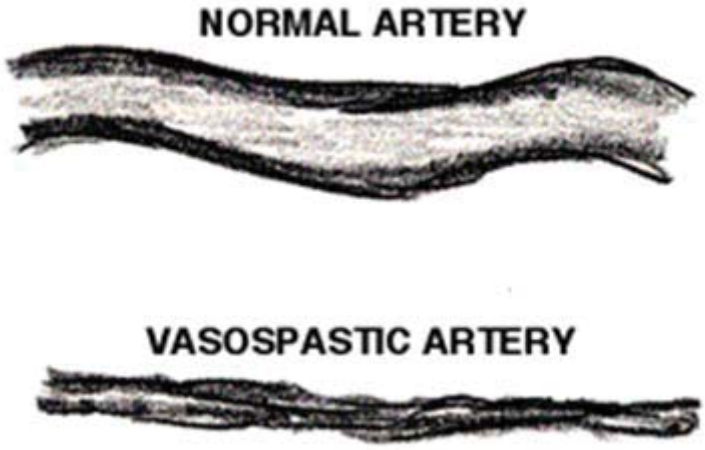

Figure 2: Vasoconstriction
Image adapted from brain-aneurysm.com

CHAPTER 2. THE EFFECTS OF CHRONIC NEURAL IMPLANTATION ON LOCALIZED VASCULATURE

2.1 Abstract

Neural implants offer a great deal of promise to individuals who suffer from injuries or diseases which prevent the use of common prosthetic solutions. However, these devices trigger a reactive foreign body response due to tissue damage caused during implantation, leading to the generation of scar tissue as well as nearby cellular death; this causes an eventual drop in the efficacy of the implanted device, as the scar tissue changes the local impedance and nearby neurons die off or move away. Currently, research involving increasing the longevity and/or function of neural implants mainly involves treating or modifying this response, by attempting to decrease the activation of local glial cells or applying anti-inflammatory drugs such as dexamethasone (DEX) in the hopes that this will lessen the overall reactive tissue response or delay its activation. However, the glial response to the injury is not the only factor that can influence the implant's efficacy or the reactive tissue response, and the usage of a general anti-inflammatory drug such as dexamethasone without a complete understanding of the cerebral vasculature and its response to an implant over time may not be a sufficient solution.

Prior research within the Neuroprostheses Research Lab at Purdue has shown the presence of vasospasms (rapidly spasming vasculature) occasionally occurring during cerebral surgery, as well as potential vasoconstriction in areas near an implanted

electrode (unpublished data). Due to the high amount of blood flow required for normal neuronal function and survival (Cipolla, 2009), these conditions could lead to local cell death beyond what is already caused by apoptosis or damage due to the reactive tissue response. In this paper we attempt to quantify cerebral vasculature in mice at specific time points post implantation in order to characterize the vascular response to electrode implantation and attempt to determine if chronic vasoconstriction, or vasospasm, occurs in areas near the implant on a regular basis. We propose that this vascular quantification will allow us to more completely characterize the foreign body response, and allow for the development of measures that further improve neural prosthetic function.

2.2 Introduction

With amputations caused by disease and injury on the rise (McGimpsey & Bradford, 2008), the research and development of prosthetics which can replace lost limbs or function continues to increase in relevance. Of the current technologies available, prosthetics which interface directly with the nervous system offer the greatest chance at a true restoration of what was lost. However, these devices still suffer from a number of challenges that need to be solved before they can be successfully utilized in the market, including signal acquisition and processing as well as electrode degradation and the reaction of local tissue to a chronic implant (Reichert, 2008). A number of these challenges stem from the foreign body response to implanted materials, as the body's reaction is to remove or segregate these materials from nearby tissue, even at the cost of local tissue destruction (Ahmed, 2011b; Qin et al., 2007b).

In the case of central interface devices implanted directly into the brain, the first steps of the foreign body response involve the release of pro-inflammatory signals from damaged cells. This in turn is followed by the dilation of nearby vasculature and the migration of immune cells into the brain through the now-compromised blood brain barrier, as well as the migration of local microglial cells towards the site of injury. Over time, astrocytes will migrate towards the site of injury following signaling from microglia, and begin to form a sheath surrounding the implant in an attempt to restore the blood brain barrier's integrity (Turner et al., 1999). This process can take a number of weeks to accomplish, but can begin influencing the ability of the implant to stimulate and record from local neurons within 7 days (Reichert, 2008). In addition to the changes in impedance caused by the process of astrogliosis, there is a region surrounding the implant where studies have shown a decrease in the neuronal density (Biran, Martin, & Tresco, 2005; Edell, Toi, McNeil, & Clark, 1992), leading to further deficits in the implant's ability to function. There have been many attempts to deal with the symptoms of chronic implantation, with studies targeting different aspects of the response being met with various degrees of success (He & Bellamkonda, 2005; Marin & Fernández, 2010). Some of these include modifications to the implant itself, such as changes to the implant's structure to minimize damage caused during insertion (Kozai et al., 2012; Seymour & Kipke, 2007) and the addition of various coatings in order to prevent the adhesion of glial cells or to decrease the impedance (Marin & Fernández, 2010). Other attempts to increase the longevity of chronic neural implants include application of DC current in order to remove glial scarring already present and covering the electrode sites, as well as treatment using anti-

inflammatory drugs in order to try and decrease cellular activation in response to injury (Nemati et al., 2013).

With the inflammatory response playing such an important role in the tissue response to an implant, understanding trends in how local blood vessels change after implantation is an important towards a more accurate quantification of the foreign body response. While too much vasodilation in response to the injury can lead to damaging consequences for local tissue, too much vasoconstriction in the area can lead to similarly damaging states. With previous research showing vasospasms occurring during electrode implantation as well as apparent vasoconstriction near an implant at a chronic time point, we decided to investigate the potential for vasoconstriction in the vasculature surrounding the implant. For this experiment, we hypothesized that the vasculature local to the implant would undergo vasoconstriction by up to 7 days post implantation, and that vasculature in the hemisphere of the brain opposite the site of injury would have no changes in vascular diameter.

2.3 Materials and Methods

2.3.1 Animals

All animals used in this study were handled in accordance to the ethical treatment of animals guidelines from the Purdue Animal Care and Use Committee (PACUC). The animals utilized in this study were transgenic mice originating from the University of Wisconsin, but a similar strain is now available from JAX. The strain these animals belong to is titled CX3CR1-GFP due to the insertion of a GFP sequence following the

promoter for CX3CR1, a transmembrane protein shown to be present in monocyte derived immune cells present in the periphery and central nervous system which also plays a part in microglial activation and migration (Jung et al., 2000). By using these mice for our experiment it allows us to monitor the location and morphology of microglial cells in the brain, as well as potentially allowing us to image immune cells from the periphery that are migrating to the site of injury. Through monitoring microglial activation in response to penetrating injury alongside the vascular response, we hope to be able to determine relationships between the two aspects of the reactive tissue response while also setting baseline values for future research. 14 animals at 2 months of age were used in the study, with 12 of them surviving surgery. This gave us 4 animals to be sacrificed at 0 (30 minutes – 1 hour following initial implant), 3, and 7 days post implantations.

2.3.2 Surgery

Surgeries were performed using the Purdue Neuroprostheses Research Lab's standard anesthesia protocol (Andrew J Woolley, Desai, Steckbeck, Patel, & Otto, 2011), which utilizes isoflurane anesthesia during surgery with a follow-up meloxicam analgesic post-surgery. Michigan shank dummy electrodes were affixed to metal rods and were cleaned prior to application through plasma sterilization via Sterrad. Other surgical articles required for surgery were sterilized via autoclave.

To begin, the heads were shaved and cleaned with betadine and ethanol following the application of a stereotaxic setup. Injection of lidocaine below the scalp was performed prior to the incision for localized anesthesia – after the initial incision, blunt dissection of

the periosteum was used to expose the skull. Craniotomies were drilled posterior to the bregma, and then electrodes were affixed to an automated insertion device. The implantations were performed utilizing a computer controlled insertion rig to control for the depth and force applied to the implant during insertion, as varying the insertion rate can change the amount of cerebral damage caused during implantation (Bjornsson et al., 2006). Electrodes were inserted 2mm into the cortex at a rate of 1mm/s, and then clipped from the insertion rig using scissors to allow for closing of the craniotomy. Following implantation, Gelfoam was used to pack the craniotomy, with a series of follow-up applications of UV dental acrylic in order to seal the region and minimize confounding factors including further foreign material contamination or brain exposure. Animals were then taken off isoflurane, and placed on oxygen until they recovered normal locomotion ability. Animals received injections of meloxicam diluted in saline each day for 3 days following surgery to minimize stress and pain following surgery.

2.3.3 Perfusion

Animals were sacrificed at 0, 3, and 7 day time points after surgery in order to examine the course of vascular response to injury within a time frame already well characterized in microglial and astrocyte activation. Previous research has shown that the blood brain barrier is disrupted immediately after cerebral damage (A.J. Woolley, Desai, Gaire, Ready, & Otto, 2013), but the overall cellular response is slightly delayed from the onset of the injury. Sacrifice was performed via isoflurane anesthesia followed by PBS and 4% PFA transcardial perfusion and head removal. In order to prevent vessel dilation and damage from occurring during perfusion, special care was taken to keep the perfusion

pressure at or below physiological levels 120 mm Hg (Mattson, 2001). Heads were soaked in 4% PFA to facilitate tissue fixation overnight, followed by three 4 hour washes of PBS to remove excess paraformaldehyde. Brains were extracted via rangiers and then sliced using a vibratome along the coronal plane, following the previously published Device Capture Histology (DCHIST) protocol (Andrew J Woolley, Desai, Gaire, Ready, & Otto, 2013).

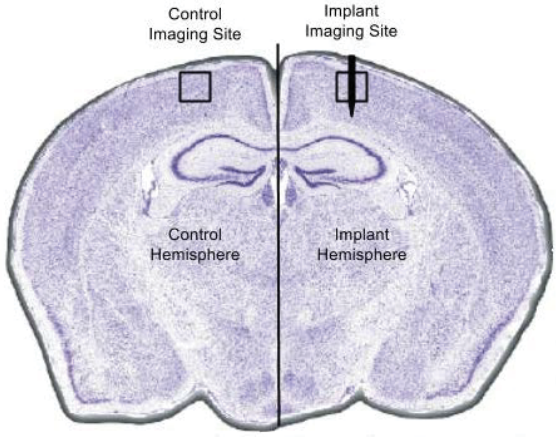

Figure 3: Brain Diagram
Example image of brain slice containing implant. Brain image from 3D VisionSoft MiceSlice program.

2.3.4 Histology

Staining was accomplished using the Purdue Neuroprostheses Research Lab standard histology protocol: primary and secondary antibodies are incubated consecutively at 4 degrees Celsius for 48 hours each, with multiple washes before and after in order to remove excess antibodies. The wash solution used in the procedure is composed of 1%/1% Volume/Volume Normal Goat Serum and .3% Triton X-100 in HEPES buffered Hank's Saline with Sodium Azide (HBHS). The specifics of the procedure are detailed in Table 1.

Table 1: Staining Protocol

Washing/Blocking	Samples washed with HBHS 3 times for 5 minutes each, then blocked for two hours in wash solution. Flip after one hour.
Primary	Incubate in primary antibodies for 48 hours at 4 celsius. Flip samples after 24 hours.
Washing	Wash 6 times for 3 minutes each using wash solution. Then wash 6 times for 1 hour, flipping samples after 3 washes.
Secondary	Incubate in secondary antibodies for 48 hours at 4 celsius. Flip samples after 24 hours.
Washing	Wash 6 times for 3 minutes each using wash solution. Then wash 6 times for 1 hour, flipping samples after 3 washes.

In the experiment we utilized antibodies specific to Neuronal Nuclei (NeuN), Blood Vessels / Endothelial Cells (CD31), and Hoechst 33258 in order to stain cell nuclei and allow for the segregation of different cells. Secondary antibodies were Alexa Fluor 568 and Alexa Fluor 633, with Hoechst added during the secondary antibody application. These were diluted into the previously described wash solution: dilutions of antibody to solution were as follows:

Table 2: Sample Staining

	Neuronal Nuclei	Microglia	Blood Vessels	Nuclei
Primary	NeuN – 1:400	Endogenous	CD31 – 1:200	-
Secondary	AF 633 – 1:500	Endogenous	AF 568 – 1:300	Hoechst 33258 0.5 ug/ml

After completion of staining, samples were organized into a 24-well plate and cleared using the SeeDB clearing agent (Ke, Fujimoto, & Imai, 2013), chosen for its rapid clearing effect of brain tissue along with the minimal change in the sample size over the course of clearing. The SeeDB solution is composed of α-thiolglycerol (5 µl / ml) and various concentrations of fructose dissolved into water, and the clearing technique itself is performed by changing the SeeDB solution over the course of up to 3 days, as detailed

below. Samples submerged in SeeDB must be left at room temperature to prevent precipitation of fructose.

Table 3: SeeDB Clearing

Concentration (Wt/Volume)	Time (Hours)
20% Fructose	4-8
40% Fructose	4-8
60% Fructose	4-8
80% Fructose	12
100% Fructose	12
115% Fructose	24

Samples were then mounted between two glass coverslips in order to allow for imaging of both sides of the sample. In order to construct this mount, PDMS spacers were cut to appropriate sizes matching the thickness of the samples using a vibratome and then used in conjunction with BluTack to prevent sample damage caused by over compression during flattening of the sample and mount. Following compression, the whole mount was sealed using a bead of Kwik-Sil in order to prevent media from dissolving or leaking during extended imaging sessions, an issue we had previously encountered when imaging with the SeeDB solution as a mounting media. A diagram of the mount, along with a picture of the actual mount in use, is shown in Figure 4.

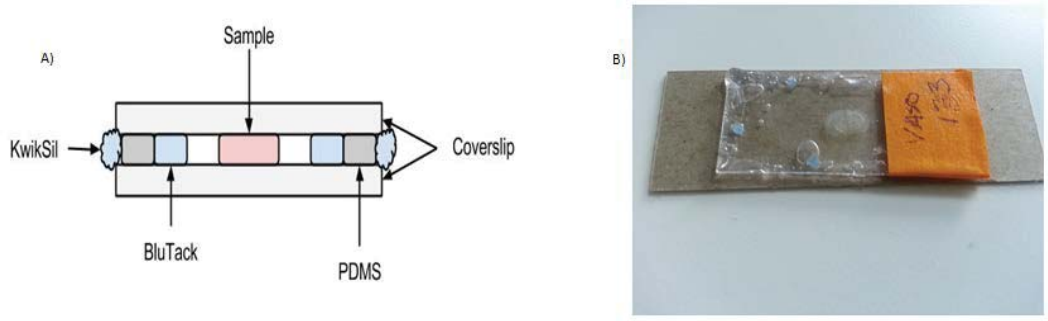

Figure 4: Sample Mounting
(A) A schematic of the prep utilized to image from both sides of the sample. (B) Mount in use.

2.3.5 Imaging

Brain slices were imaged using a Zeiss LSM 710 inverted confocal microscope, using the Smart Setup controls to automatically generate the correct settings (Hoechst 33528, EGFP, Atto-555, AlexaFluor-633). Laser lines were broken into two separate tracks to minimize cross-talk: 405nm & 633nm, 488nm & 561nm. Each of these combinations has sufficiently separated excitation and emission spectra that they can be imaged at once, in order to save time. Images were taken using a 25x Oil objective at .7 zoom, a pinhole of 1 AU, and a Z step size of 1.13 microns to create 486 x 486 x 250 micron dimension image stacks of tissue. Images are taken at 2048 x 2048 pixels, giving us 4.216 pixels per micron. These dimensions allow for the collection of imaging data wholly containing a portion of the implant as well as nearby tissue. DCHIST slices were imaged four times, twice on either side on both the control (undamaged) hemisphere and the hemisphere containing the electrode.

2.3.6 Post-Processing and Quantification

Z-stack image files were then imported into FIJI (Schindelin et al., 2012), an open source image processing suite, for post-processing. Channel separation and vessel identification were performed using a macro utilizing features already included in the program, with a separate macro/function written for vessel quantification. A flowchart detailing the basics of this method is shown in Figure 5, and the current version of the code is contained in the Appendix. In order to save time and efficiently process the data, each Z level is processed separately by the cleaning software. The macro first loads one plane of the image, then runs Gaussian Blur at a sigma value of 1. After the blur, the Tubeness function is used to segment cylindrical structures from the image. At completion of the single Z plane, the file is saved and then a new plane is loaded – this continues until the entire image sequence has been processed. The series is then repeated again at a sigma value increased by 1 (1 , 2, 3, 4, and 5 values for sigma were used in this project) . After completion of all sigma values, images are then added together in order to create one composite image. The variation of the sigma values allows for the macro to extract vessels with various diameters, allowing us to characterize all the vasculature rather than a subsection of it.

Following the completion of the averaged image, the user decides on a threshold setting and runs Connected Regions to remove structures smaller than a certain size. The file output by this process must be converted to binary in order to facilitate the next quantification step. The second macro contained utilizes the Skeletonize plugin to erode vessels down to their centerlines; this data is then loaded into a modified Analyze Skeleton plugin in order to extract data about the vessel. By selecting each vessel with a

wand tool and then summing the voxels contained within it on all the Z planes the structure is present in, we are able to quantify and output relevant data such as length, diameter, and beginning and end points. Vessel data was then collected into histograms based on normalized vessel diameter and time points. The normalization process is achieved by segmenting each vessel into 1 micron long sections and then counting the number of sections contained – this allows us to control for the fact that the larger vessels will contain more pixels than the smaller vessels. This mismatch in pixel amount means that calculations based just on the amount of voxels contained within each object will be skewed towards larger vessels. The data generated was used in conjunction with the Kolmogorov-Smirnov test (K-S test), in order to determine if there were statistical differences between the histograms generated in this fashion.

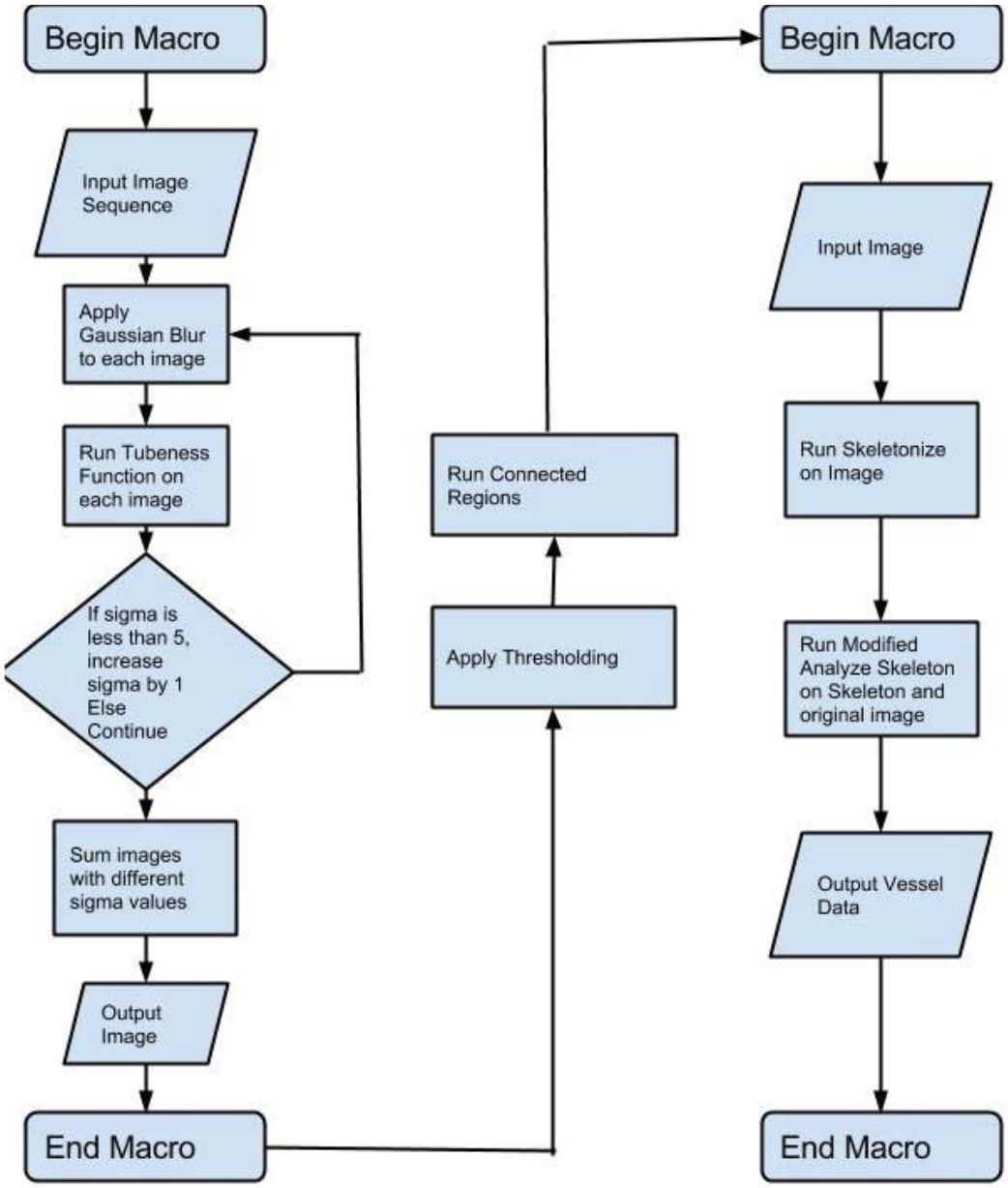

Figure 5: Post-Processing Flowchart
Flowchart detailing how the coding components function

2.4 Results

Post-processing of our images generated length and diameter values for vascular segments contained within each image. The total number of segments within each image is listed in Table 3. Within this data there is a slight trend towards a greater number of

segments calculated within the control hemisphere images. Histograms of data from time points 0, 3, and 7 day implantation are shown in figures 9, 10, and 11.

Table 4: Vascular Segments Per Image

Image Name | Time Point	Vascular Segments Control | Implant
Vaso 17 | 0 Day	268909 | 97897
Vaso 11 | 0 Day	147594 | 286996
Vaso 16 | 0 Day	690761 | 538496
Vaso 10 | 3 Day	497601 | 394994
Vaso 14 | 3 Day	585998 | 345610
Vaso 15 | 3 Day	525687 | 424891
Vaso 4 | 7 Day	471075 | 274157
Vaso 5 | 7 Day	514705 | 334036
Vaso 8 | 7 Day	715861 | 730091

Unprocessed maximum projection images of microglial, vascular, and neuronal signal are shown in figures 7, 8, 9. Examination of the microglial images show activation by day 3, as cell bodies enlarge and processes shorten, and apparent migration by day 7, where the distribution of microglia is tightly packed around the implant site. Vasculature in the implanted region appears to be enlarged at 3 and 7 days in comparison with control images. Neuronal nuclei appear normal at 0 days implanted, but their morphology in regions surrounding the implant appears to elongate and shrink by 3 days implanted. This shift in morphology is less apparent by 7 days implanted.

After running the Kolmogorv-Smirnov Test with $\alpha = 0.05$, results show that control data and implant data have statistical differences between them and cannot be drawn from the same continuous distribution. The results also indicate that the different control hemispheres between animals and time-points cannot be drawn from the same distribution, as the K-S test rejects the null hypothesis when comparing the various

datasets. In order to explore this, median data from each distribution was used to determine trends in both control and implant hemispheres as the time implanted increases (Figure 12). This comparison shows an increase in the control vascular diameter median over time, going from 3.82 μm initially to 4.31 by 7 days implanted. It also shows an increase and subsequent decrease in the vascular diameter of the region surrounding the implant: the vessel median begins at 3.26 μm, goes up to 5.58 μm by 3 days of implantation, and drops down to 5.12 μm by 7 days. This matches with the overall trends shown in figures 9-11, with similar vascular distributions at 0 days implanted, wider distributions of vasculature

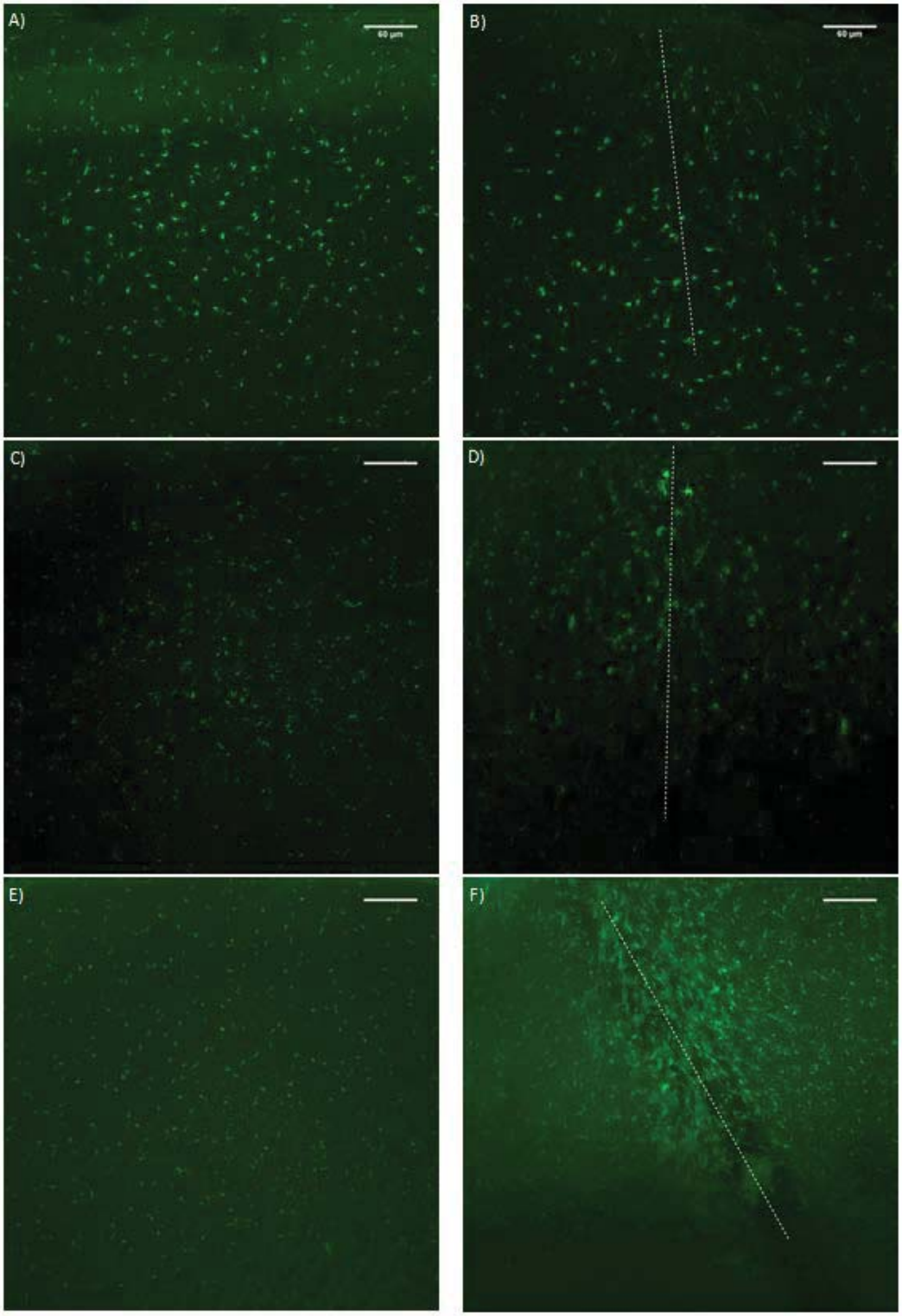

Figure 6: Microglial Comparison
Images A, C, and E are representative images of the control hemispheres at 0, 3, and 7 day time points. Images B, D, and F show implanted hemispheres at the same time points. The dotted line represents the location of the implant. All images are of microglia, at 488 nm wavelength. Scale bar is 60 μm in length.

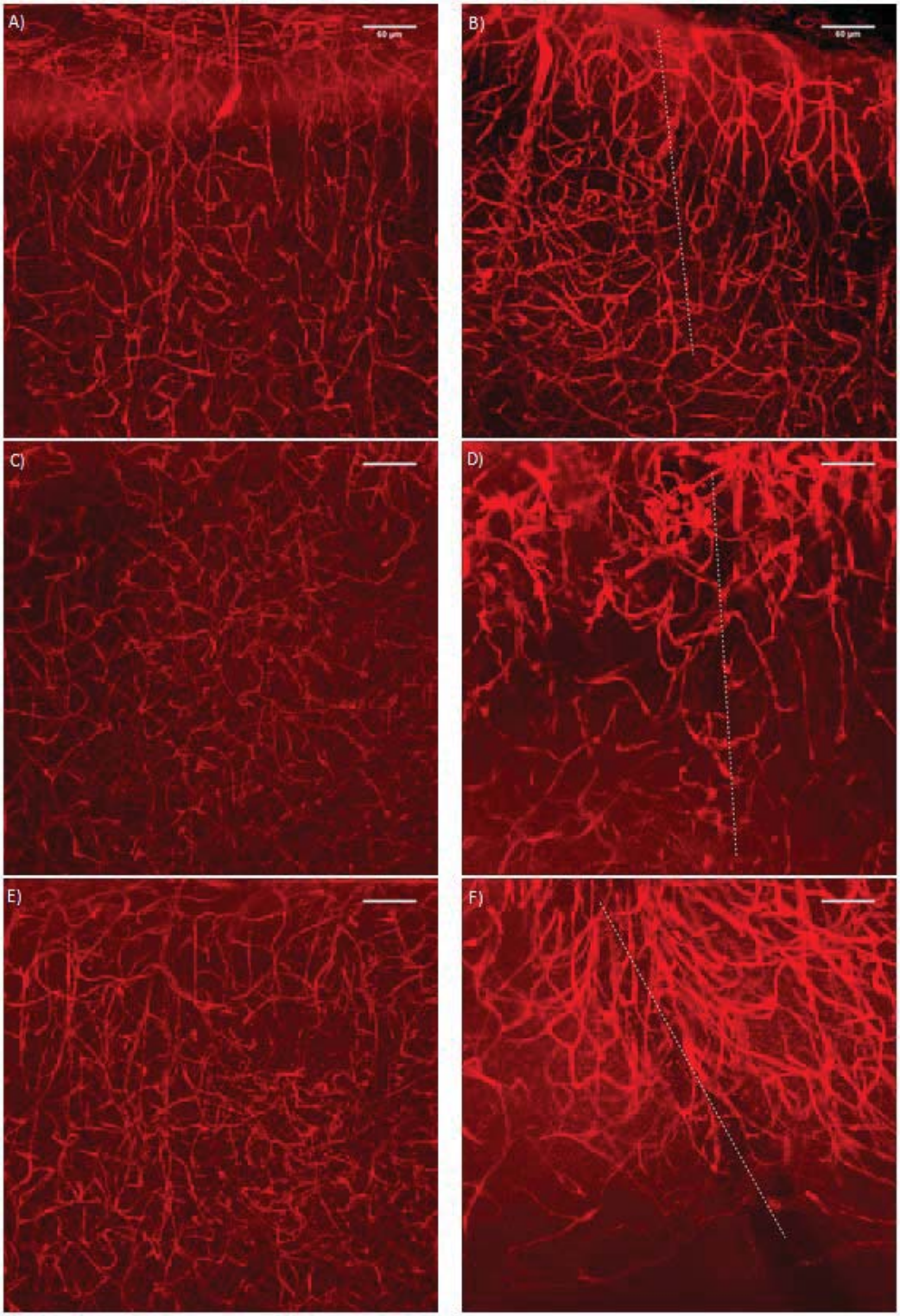

Figure 7: Vascular Comparison
Images A, C, and E are representative images of the control hemispheres at 0, 3, and 7 day time points. Images B, D, and F show implanted hemispheres at the same time points. The dotted line represents the location of the implant. All images are of vasculature, at 561 nm wavelength. Scale bar is 60 μm in length.

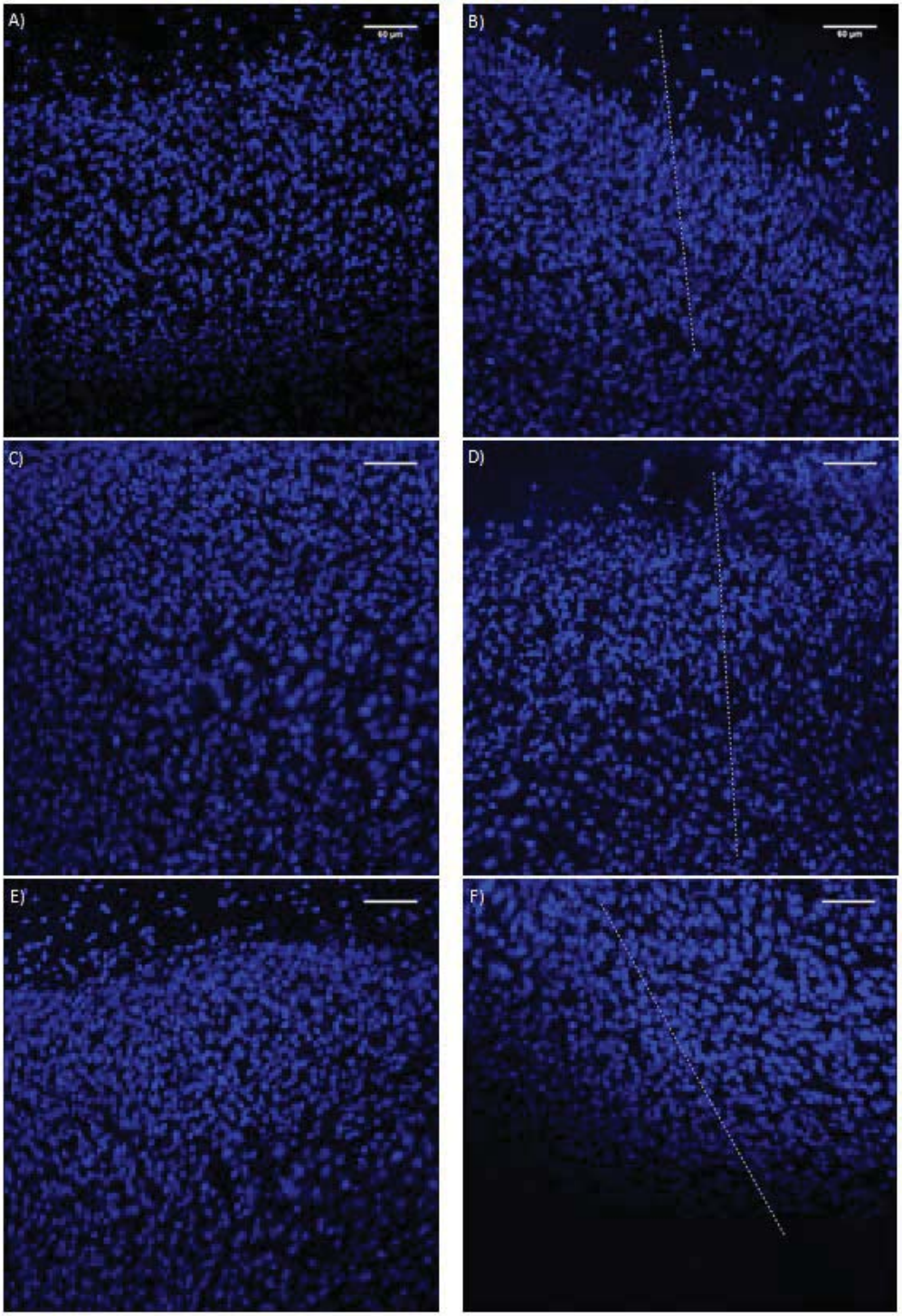

Figure 8: Neuronal Comparison
Images A, C, and E are representative images of the control hemispheres at 0, 3, and 7 day time points. Images B, D, and F show implanted hemispheres at the same time points. The dotted line represents the location of the implant. All images are of neuronal nuclei, at 633 nm wavelength. Scale bar is 60 μm in length.

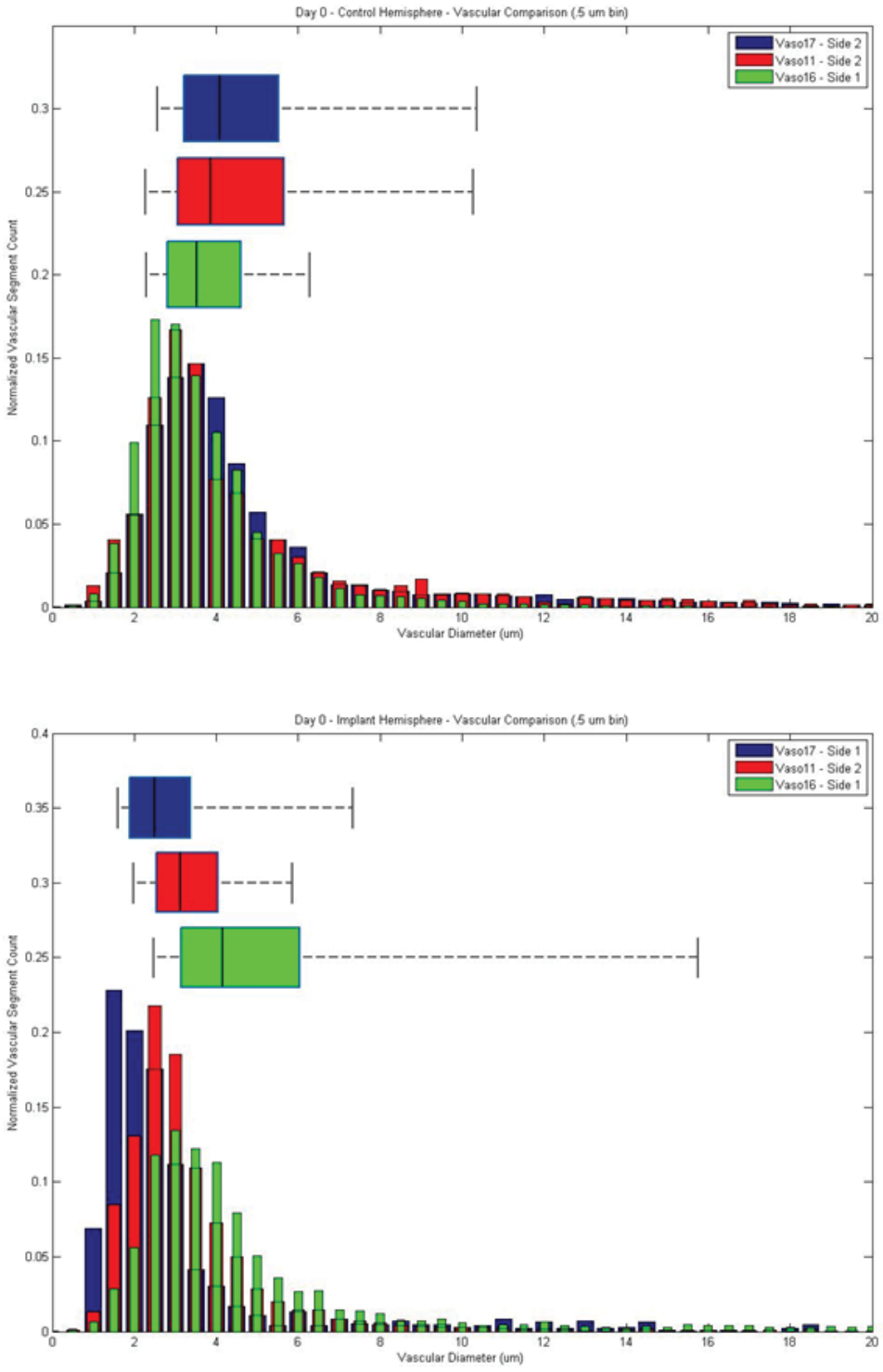

Figure 9: Day 0 comparison of Control and Implant data.

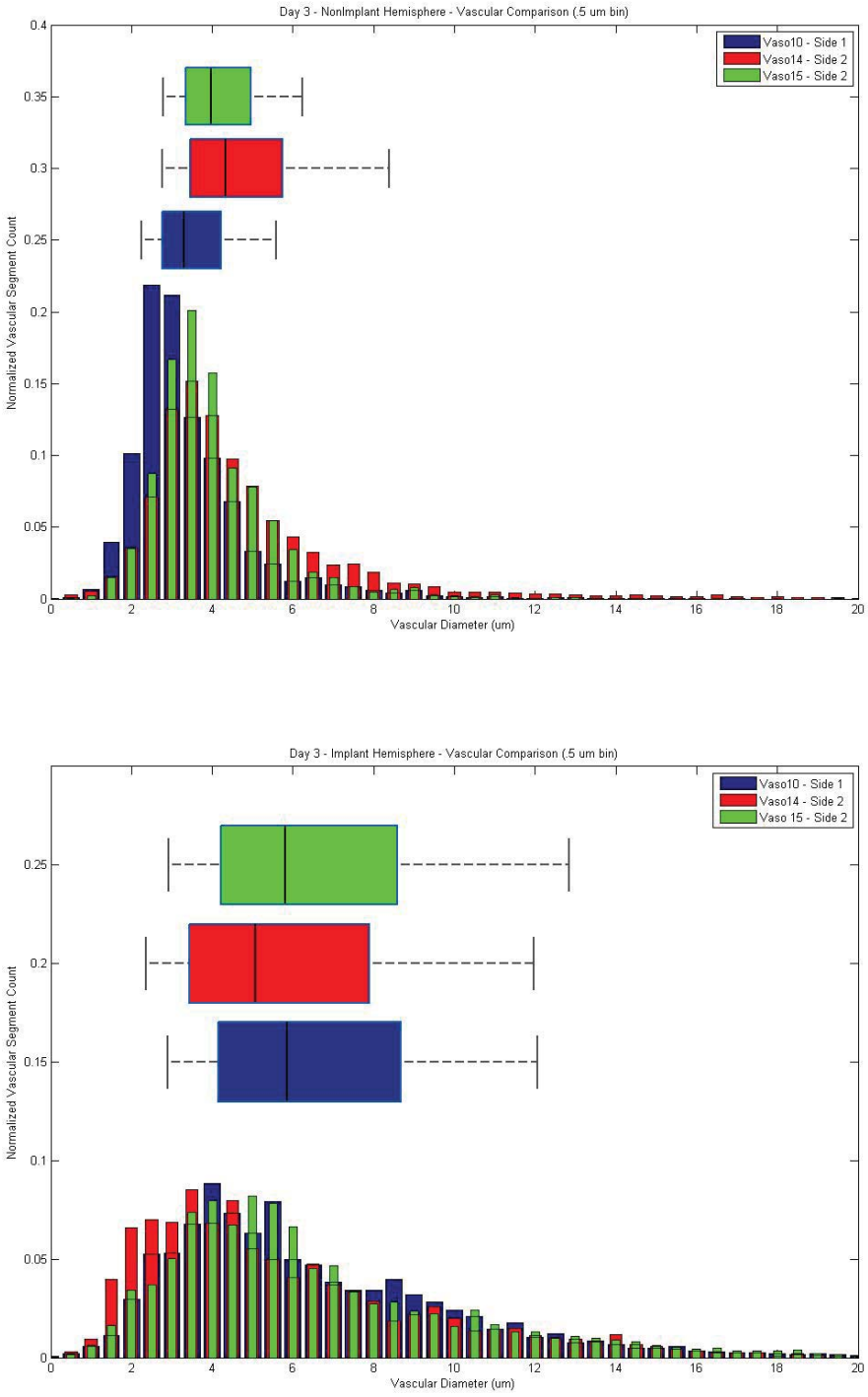

Figure 10: Day 3 comparison of Control and Implant data.

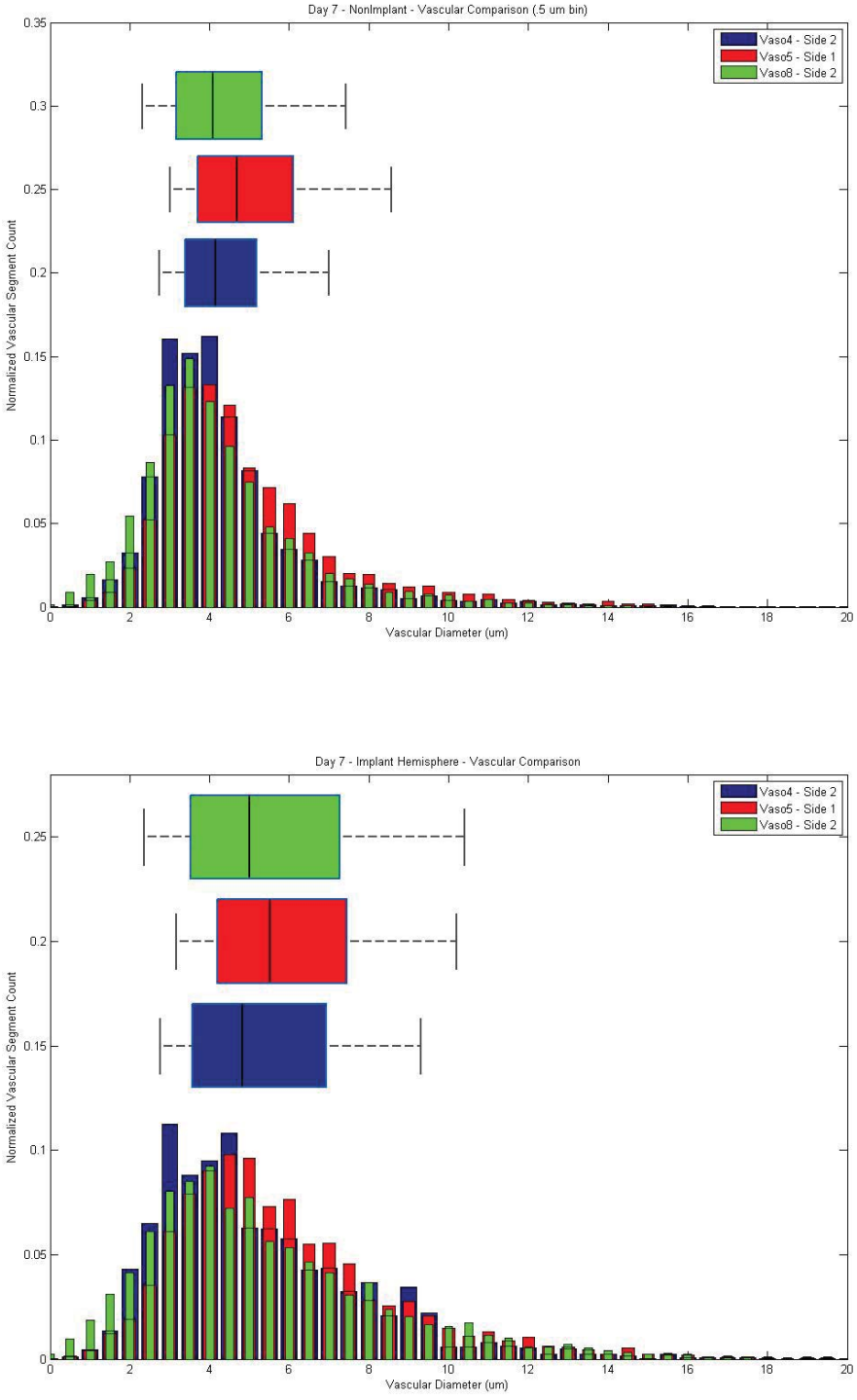

Figure 11: Day 7 comparison of Control and Implant data.

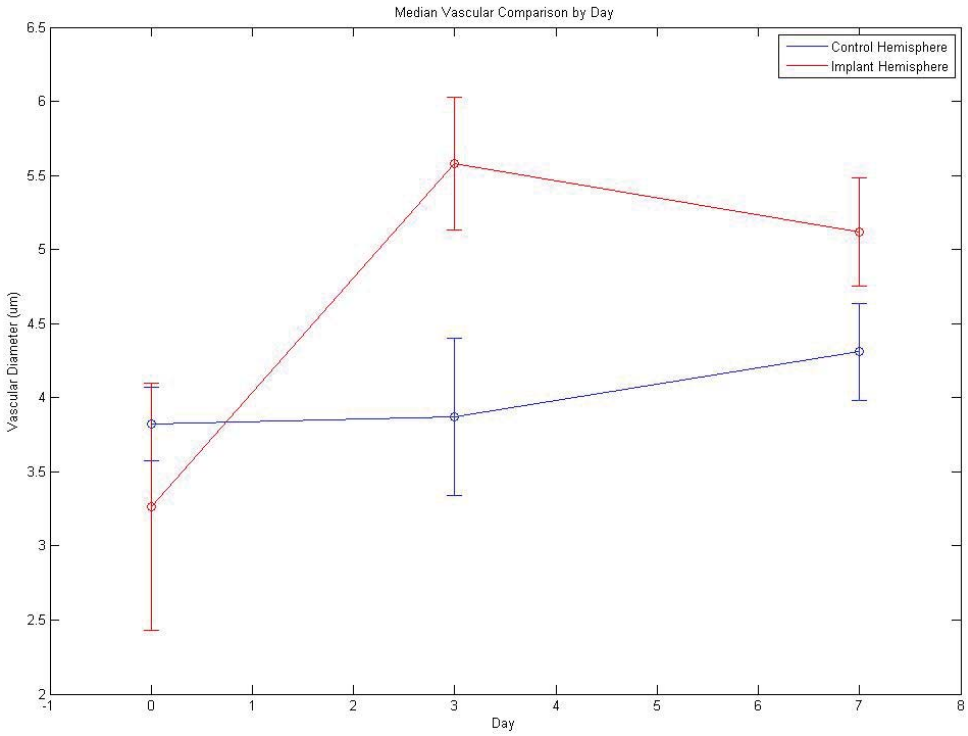

Figure 12: Comparison of median vascular diameter.
Median vascular diameter in control and implant hemispheres at 0, 3, and 7 day time points. Bars show standard deviation of median within samples used at each time point.

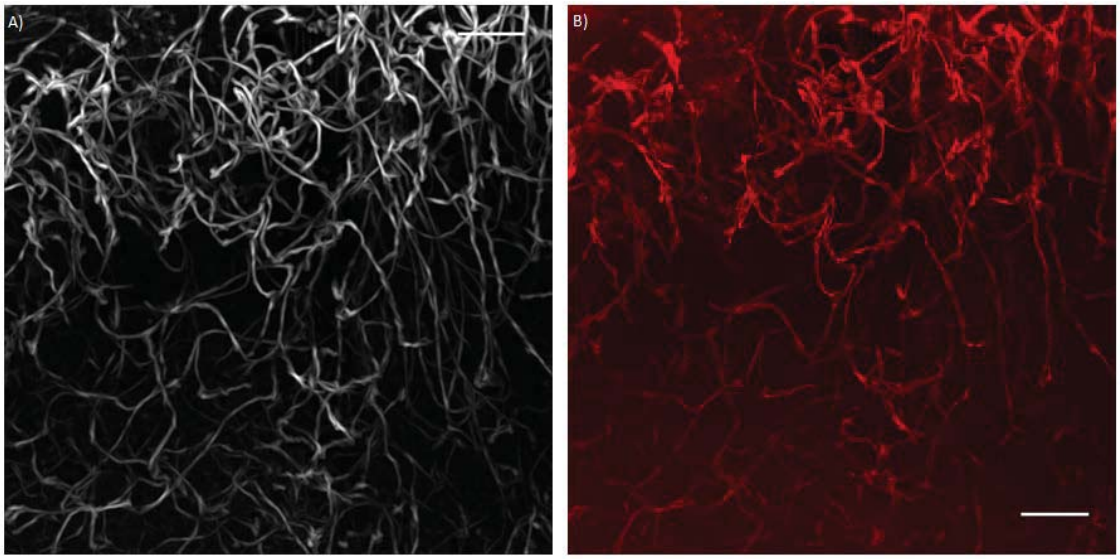

Figure 13: Processed vs Unprocessed
Comparison between processed data (A) and actual data (B). Scale bar is 60 μm in length

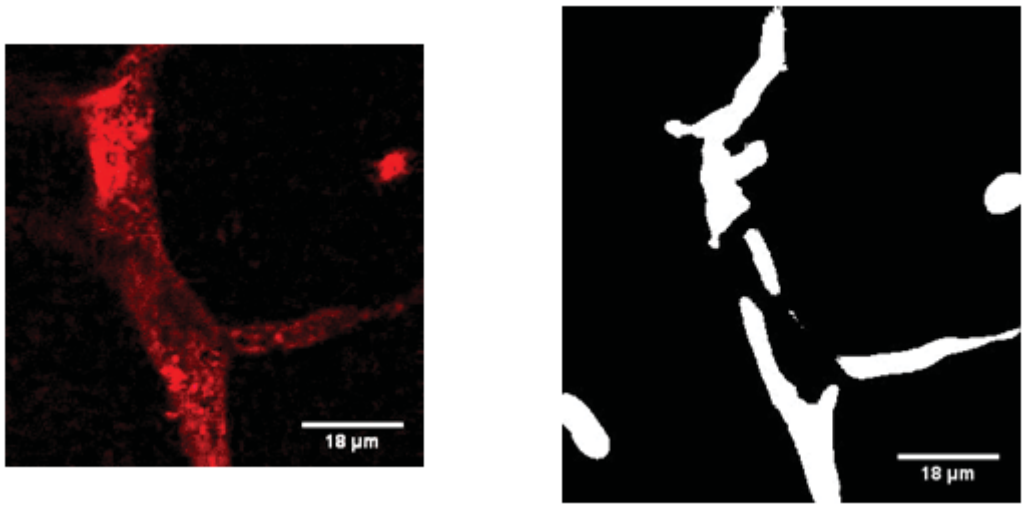

Figure 14: Fragmentation of larger vessels after post-processing

2.5 Discussion

Contradictory to our initial hypothesis, our results do not show vasoconstriction in the region surrounding the implant at up to 7 days post implantation. We were able to successfully quantify and follow trends in the dilation of blood vessels in the area surrounding the implant, but our results show vasodilation in response to the injury instead of vasoconstriction. Our results imply that the vasodilation caused by the initial injury and the inflammatory response are compensated for by day 7, when we begin to see a higher population of microglia surrounding the implant – this compensation is likely due to the local microglial activation and secretion of anti-inflammatory cytokines (Aloisi, 2001). In addition to the vasodilation occurring in the implanted region, our data suggests vasodilation in the control hemisphere over time as well. While the changes in vascular diameter are not as pronounced as those present in the implant hemisphere, this data supports previous results published showing disruption of the blood brain barrier in

the hemisphere contralateral to the initial damage; this could easily be due to vascular dilation disrupting the tight end junctions forming the blood brain barrier. The occurrence of vasoconstriction may occur after the normal vasodilation has taken its course – the abundance of anti-inflammatory secretions in combination with the disrupted ability of the brain to auto-regulate could lead to overcompensation in response to the injury.

As seen in the graphs, some of our data is skewed towards smaller vessels – while this may be due to actual vasoconstriction, it is more likely due to our processing method breaking down some larger vessels into smaller components, shown above in Figure 14. With this in mind, future processing of this data will attempt to characterize these vessels further, in order to give a more accurate description of the changes to vasculature and comparison between the control and implant hemispheres.

2.6 Future Research Directions

As we were unable to isolate any instances of vasoconstriction within the time constraints of this study, the next research goal would be to characterize the vasculature at later time points. One of the reasons for this is that an accepted time point for when the acute portion of the foreign body response resolves is at a month in – if vasoconstriction occurs at or after this time point, it could influence the local neuronal population further and degrade the function of a neuronal implant. This vasoconstriction could be due to a continued disruption of the auto-regulatory properties of the local vasculature due to the continued presence of an implant, an overabundance of anti-inflammatory signaling from activated glial cells nearby, or even vasoconstriction due to a lessened metabolic need caused by local cell death. Other goals may involve characterizing the vasculature using

the same method in response to anti-inflammatory drugs or treatment, in an attempt to discover how this influences the dilation or constriction of local vasculature over time, and what consequences may occur due to modifying the brain's auto-regulatory capabilities. Of particular interest for this research would be utilizing a window applied over a craniotomy for in-vivo characterization of the vascular response to injury; this allows for real time quantification of live vasculature, which would allow for a more accurate characterization and understanding of vasodilation or constriction and when it occurs. Characterization of the links between astrocytes, vascular changes, and the blood brain barrier would also be useful to quantify, as completely understanding this relationship is an important step towards maintaining implant function while also keeping the brain healthy.

2.7 Conclusions

In the case of vasculature and its part in the inflammatory and foreign body responses, vasoconstriction and vasodilation are two faces of the same coin. Both of these conditions can cause severe damage to local tissue and the brain if left unchecked, but are also necessary for normal function and as a result are tightly regulated in a healthy brain. The loss of the auto-regulatory control following injury is concerning, and has the potential to cause damage to nearby tissue in normally innocuous situations that would be compensated for normally. In this study, we were able to characterize vasodilation at up to 7 days post implantation, along with data indicating the occurrence of vasodilation in the opposite hemisphere where no damage had occurred. The vasodilation in the opposite

hemisphere could be an attempt to compensate for the damaged hemisphere, or even trying to compensate for the disrupted vascular regulation on the damage side.

Quantification of vasculature and other forms of tube-like networks, including neurons, is a difficult thing to accomplish, and is at best only partially automated. Unlike previous methods which utilize human input to determine the beginning and end of a segment of vasculature or neuron, our methodology is able to isolate and quantify tube-like structures on its own, only necessitating human input currently to get the most accurate skeleton through thresholding. By utilizing this technique, it may become easier to setup data-processing pipelines and facilitate the rapid quantification of connected networks without human intervention.

In conclusion, our techniques in both imaging and post-processing allow us to quantify the diameter and length of vasculature present in the cortex while only using standard histological methods. The results we collected follow along the trends seen previously with the vascular response to implantation. These results show that we can quantify the effects on vasculature without having to resort to complicated surgical preps or expensive microscopy solutions, and allows for future research to quantify the vascular response in a fast and cost-efficient method.

BIBLIOGRAPHY

BIBLIOGRAPHY

Ahmed, A. U. (2011a). An overview of inflammation: mechanism and consequences. *Frontiers in Biology*, *6*(4), 274–281. doi:10.1007/s11515-011-1123-9

Aloisi, F. (2001). Immune function of microglia. *Glia*, *36*(2), 165–79. Retrieved from http://www.ncbi.nlm.nih.gov/pubmed/11596125

American Diabetes Association. (2005). Peripheral Arterial Disease in People with Diabetes. *Journal of the American Podiatric Medical Association*, *95*, 309–319.

Anderson, J. (1988). Inflammatory response to implants. *ASAIO Journal*. Retrieved from http://journals.lww.com/asaiojournal/Abstract/1988/04000/Inflammatory_Response_to_Implants.5.aspx

Anderson, J. M., Rodriguez, A., & Chang, D. T. (2008). Foreign body reaction to biomaterials. *Seminars in Immunology*, *20*(2), 86–100. doi:10.1016/j.smim.2007.11.004

Attwell, D., Buchan, A. M., Charpak, S., Lauritzen, M., Macvicar, B. A., & Newman, E. A. (2010). Glial and neuronal control of brain blood flow. *Nature*, *468*(7321), 232–43. doi:10.1038/nature09613

Becher, B., Prat, A., & Antel, J. P. (2000). Brain-immune connection: immuno-regulatory properties of CNS-resident cells. *Glia*, *29*(4), 293–304. Retrieved from http://www.ncbi.nlm.nih.gov/pubmed/10652440

Benabid, A. L. (2003). Deep brain stimulation for Parkinson's disease. *Current Opinion in Neurobiology*, *13*(6), 696–706. doi:10.1016/j.conb.2003.11.001

Biran, R., Martin, D. C., & Tresco, P. A. (2005). Neuronal cell loss accompanies the brain tissue response to chronically implanted silicon microelectrode arrays. *Experimental Neurology*, *195*(1), 115–26. doi:10.1016/j.expneurol.2005.04.020

Bjornsson, C. S., Oh, S. J., Al-Kofahi, Y. A., Lim, Y. J., Smith, K. L., Turner, J. N., … Kim, S. J. (2006). Effects of insertion conditions on tissue strain and vascular damage during neuroprosthetic device insertion. *Journal of Neural Engineering*, *3*(3), 196–207. doi:10.1088/1741-2560/3/3/002

Call, G. K., Fleming, M. C., Sealfon, S., Levine, H., Kistler, J. P., & Fisher, C. M. (1988). Reversible cerebral segmental vasoconstriction. *Stroke*, *19*(9), 1159–1170. doi:10.1161/01.STR.19.9.1159

Chang, H.-T. (1951). DENDRITIC POTENTIAL OF CORTICAL NEURONS PRODUCED BY DIRECT ELECTRICAL STIMULATION OF THE CEREBRAL CORTEX. *J Neurophysiol*, *14*(1), 1–21. Retrieved from http://jn.physiology.org/content/14/1/1

Cipolla, M. (2009). Control of Cerebral Blood Flow. In *The Cerebral Circulation*. Morgan & Claypool Life Sciences. Retrieved from http://www.ncbi.nlm.nih.gov/books/NBK53082/

Edell, D. J., Toi, V. V, McNeil, V. M., & Clark, L. D. (1992). Factors influencing the biocompatibility of insertable silicon microshafts in cerebral cortex. *IEEE Transactions on Bio-Medical Engineering*, *39*(6), 635–43. doi:10.1109/10.141202

Hafner, B. J., Willingham, L. L., Buell, N. C., Allyn, K. J., & Smith, D. G. (2007). Evaluation of function, performance, and preference as transfemoral amputees transition from mechanical to microprocessor control of the prosthetic knee. *Archives of Physical Medicine and Rehabilitation*, *88*(2), 207–17. doi:10.1016/j.apmr.2006.10.030

Haynes, D. S., & Labadie, R. F. (2000). Making The Deaf Hear Cochlear Implantation, 8–12.

He, W., & Bellamkonda, R. V. (2005). Nanoscale neuro-integrative coatings for neural implants. *Biomaterials*, *26*(16), 2983–90. doi:10.1016/j.biomaterials.2004.08.021

Janjua, N., & Mayer, S. A. (2003). Cerebral vasospasm after subarachnoid hemorrhage. *Current Opinion in Critical Care*, *9*(2), 113–9. Retrieved from http://www.ncbi.nlm.nih.gov/pubmed/12657973

Jung, S., Aliberti, J., Graemmel, P., Sunshine, M. J., Kreutzberg, G. W., Sher, A., & Littman, D. R. (2000). Analysis of fractalkine receptor CX(3)CR1 function by targeted deletion and green fluorescent protein reporter gene insertion. *Molecular and Cellular Biology*, *20*(11), 4106–14. Retrieved from http://www.pubmedcentral.nih.gov/articlerender.fcgi?artid=85780&tool=pmcentrez&rendertype=abstract

Ke, M.-T., Fujimoto, S., & Imai, T. (2013). SeeDB: a simple and morphology-preserving optical clearing agent for neuronal circuit reconstruction. *Nature Neuroscience*, *16*(8), 1154–1161. doi:10.1038/nn.3447

Kozai, T. D. Y., Langhals, N. B., Patel, P. R., Deng, X., Zhang, H., Smith, K. L., … Kipke, D. R. (2012). Ultrasmall implantable composite microelectrodes with bioactive surfaces for chronic neural interfaces. *Nature Materials*, *11*(12), 1065–73. doi:10.1038/nmat3468

Krames, E. S., Peckham, H. P., & Rezai, A. R. (Eds.). (2009). *Neuromodulation* (p. 1200). Academic Press. Retrieved from http://books.google.com/books?id=v-ks7D_Z3O8C&pgis=1

Kuiken, T. a, Dumanian, G. a, Lipschutz, R. D., Miller, L. a, & Stubblefield, K. a. (2004). The use of targeted muscle reinnervation for improved myoelectric prosthesis control in a bilateral shoulder disarticulation amputee. *Prosthetics and Orthotics International*, *28*(3), 245–53. Retrieved from http://www.ncbi.nlm.nih.gov/pubmed/15658637

Kuiken, T., Miller, L., & Lipschutz, R. (2007). Targeted reinnervation for enhanced prosthetic arm function in a woman with a proximal amputation: a case study. *The Lancet*. Retrieved from http://www.sciencedirect.com/science/article/pii/S0140673607601937

Kumar, V., Abbas, K. A., & Aster, J. (2003). *Robbins Basic Pathology, 9th ed* (9th ed., p. 928). Retrieved from https://www.inkling.com/store/book/robbins-basic-pathology-kumar-abbas-aster-9th/?chapterId=4eca681364e34e9c9de63067aca4f513

Landis, D. M. (1994). The early reactions of non-neuronal cells to brain injury. *Annual Review of Neuroscience*, *17*, 133–51. doi:10.1146/annurev.ne.17.030194.001025

Lotfi, P. (2007). *Foreign Body Reactions to Neural Implants in the Brain* (p. 89). ProQuest. Retrieved from http://books.google.com/books?id=S43zYGmrLEQC&pgis=1

Marin, C., & Fernández, E. (2010). Biocompatibility of intracortical microelectrodes: current status and future prospects. *Frontiers in Neuroengineering*, *3*, 8. doi:10.3389/fneng.2010.00008

Mattson, D. L. (2001). Comparison of arterial blood pressure in different strains of mice. *American Journal of Hypertension*, *14*(5 Pt 1), 405–8. Retrieved from http://www.ncbi.nlm.nih.gov/pubmed/11368457

McFarland, D. J., & Wolpaw, J. R. (2011). Brain-Computer Interfaces for Communication and Control. In *Communications of the ACM* (Vol. 54, pp. 60–66). doi:10.1145/1941487.1941506

McGimpsey, G., & Bradford, T. (2008). Limb Prosthetics Services and Devices. *White Paper*, 1–35. Retrieved from http://www.glb.nist.gov/tip/wp/pswp/upload/239_limb_prosthetics_services_devices.pdf

Morganti-Kossmann, M., Rancan, M., Stahel, P., & Kossmann, T. (2002). Inflammatory response in acute traumatic brain injury: a double-edged sword. *Current Opinion in Critical Care*.

Nemati, P., Imani, M., Farahmandghavi, F., Mirzadeh, H., Marzban-Rad, E., & Nasrabadi, A. M. (2013). Dexamethasone-releasing cochlear implant coatings: application of artificial neural networks for modelling of formulation parameters and drug release profile. *The Journal of Pharmacy and Pharmacology*, *65*(8), 1145–57. doi:10.1111/jphp.12086

Newby, A. C. (2000). An overview of the vascular response to injury: a tribute to the late Russell Ross. *Toxicology Letters*, *112-113*, 519–529. doi:10.1016/S0378-4274(99)00212-X

Ott, K., Serlin, D. H., & Mihm, S. (Eds.). (2002). *Artificial Parts, Practical Lives: Modern Histories of Prosthetics* (p. 359). NYU Press. Retrieved from http://books.google.com/books?hl=en&lr=&id=TkpDIrM7848C&pgis=1

Paulson, O. B., Strandgaard, S., & Edvinsson, L. (1990). Cerebral autoregulation. *Cerebrovascular and Brain Metabolism Reviews*, *2*(2), 161–92. Retrieved from http://europepmc.org/abstract/MED/2201348

Perlmutter, J. S., & Mink, J. W. (2006a). Deep brain stimulation. *Annual Review of Neuroscience*, *29*, 229–57. doi:10.1146/annurev.neuro.29.051605.112824

Perlmutter, J. S., & Mink, J. W. (2006b). Deep brain stimulation. *Annual Review of Neuroscience*, *29*, 229–57. doi:10.1146/annurev.neuro.29.051605.112824

Pibarot, P., & Dumesnil, J. G. (2009). Prosthetic heart valves: selection of the optimal prosthesis and long-term management. *Circulation*, *119*(7), 1034–48. doi:10.1161/CIRCULATIONAHA.108.778886

Polikov, V. S., Tresco, P. a, & Reichert, W. M. (2005). Response of brain tissue to chronically implanted neural electrodes. *Journal of Neuroscience Methods*, *148*(1), 1–18. doi:10.1016/j.jneumeth.2005.08.015

Potter, K. A., Buck, A. C., Self, W. K., & Capadona, J. R. (2012, August 1). Stab injury and device implantation within the brain results in inversely multiphasic neuroinflammatory and neurodegenerative responses - Abstract - Journal of Neural Engineering - IOPscience. IOP Publishing. Retrieved from http://m.iopscience.iop.org/1741-2552/9/4/046020/pdf/1741-2552_9_4_046020.pdf

Qin, L., Wu, X., Block, M. L., Liu, Y., Breese, G. R., Hong, J.-S., … Crews, F. T. (2007a). Systemic LPS causes chronic neuroinflammation and progressive neurodegeneration. *Glia*, *55*(5), 453–462. doi:10.1002/glia.20467

Qin, L., Wu, X., Block, M. L., Liu, Y., Breese, G. R., Hong, J.-S., … Crews, F. T. (2007b). Systemic LPS causes chronic neuroinflammation and progressive neurodegeneration. *Glia*, *55*(5), 453–62. doi:10.1002/glia.20467

Reichert, W. M. (Ed.). (2008). *Indwelling Neural Implants*. CRC Press. Retrieved from http://www.ncbi.nlm.nih.gov/books/NBK1977/

Sattar, A., Manousakis, G., & Jensen, M. B. (2010). Systematic review of reversible cerebral vasoconstriction syndrome. *Expert Review of Cardiovascular Therapy*, *8*(10), 1417–21. doi:10.1586/erc.10.124

Schindelin, J., Arganda-Carreras, I., Frise, E., Kaynig, V., Longair, M., Pietzsch, T., … Cardona, A. (2012). Fiji: an open-source platform for biological-image analysis. *Nature Methods*, *9*(7), 676–82. doi:10.1038/nmeth.2019

Seymour, J. P., & Kipke, D. R. (2007). Neural probe design for reduced tissue encapsulation in CNS. *Biomaterials*, *28*(25), 3594–607. doi:10.1016/j.biomaterials.2007.03.024

Shannon, G. F. (1979). A myoelectrically-controlled prosthesis with sensory feedback. *Medical & Biological Engineering & Computing*, *17*(1), 73–80. doi:10.1007/BF02440956

Turner, J. N., Shain, W., Szarowski, D. H., Andersen, M., Martins, S., Isaacson, M., & Craighead, H. (1999). Cerebral astrocyte response to micromachined silicon implants. *Experimental Neurology*, *156*(1), 33–49. doi:10.1006/exnr.1998.6983

Woolley, A. J., Desai, H. a, Steckbeck, M. a, Patel, N. K., & Otto, K. J. (2011). In situ characterization of the brain-microdevice interface using device-capture histology. *Journal of Neuroscience Methods*, *201*(1), 67–77. doi:10.1016/j.jneumeth.2011.07.012

Woolley, A. J., Desai, H. A., Gaire, J., Ready, A. L., & Otto, K. J. (2013). A Systemic Triple Label Strategy for Fluorescent Microscopy of Inflammation in CNS and Non-CNS Tissue. *Microscopy and Microanalysis*, *19*(S2), 196–197. doi:10.1017/S1431927613002973

Woolley, A. J., Desai, H. A., Gaire, J., Ready, A. L., & Otto, K. J. (2013). Intact histological characterization of brain-implanted microdevices and surrounding tissue. *Journal of Visualized Experiments : JoVE*, (72). doi:10.3791/50126

Zindler, E., & Zipp, F. (2010). Neuronal injury in chronic CNS inflammation. *Best Practice & Research. Clinical Anaesthesiology*, *24*(4), 551–62. doi:10.1016/j.bpa.2010.11.001

APPENDIX

APPENDIX

Cleaning Code

Runnable as a .ijm (FIJI Macro) file

```
// This short macro looks for all the files called .tif
// in a directory and preprocesses them for "tubeness"
// using sigma = 3. It currently allows you to select up to
// 4 images at the same time for concurrent processing.
di = newArray('0','0','0','0');
for (k=0; k<4; k++){
di[k] = getDirectory("Choose a Directory ");
}

for (k=0; k<4; k++){
file_names = newArray("1", "2", "3", "4", "5");
file_smaller = newArray("0");//, "1", "2", "3", "4", "5", "6", "7", "8", "9");

d = di[k];
list = getFileList(d);

File.makeDirectory(d + "/averaged/");

for (f=0; f<5; f++){
      File.makeDirectory(d + "/" + file_names[f]+ "/");
for (f1=0; f1<1; f1++){
      File.makeDirectory(d + "/" + file_names[f]+ "/" + file_smaller[f1] + "/");
for (i=0; i<list.length; i++) {
   fullName = d + list[i];
   saveName = d + "/" + file_names[f]+ "/" + file_smaller[f1] + "/" + list[i];
   sigmaName = "sigma=" + file_names[f] + "." + file_smaller[f1] + " use";
   if (endsWith(fullName, ".tif")) {
      open(fullName);
      t = getTitle();
      run("Tubeness", sigmaName);
      selectWindow("tubeness of "+t);
      dotIndex = lengthOf(saveName) - 4;
      n = substring(saveName,0,dotIndex) + ".tubes.tif";
      saveAs("Tiff", n);
      close();
      close();
   }
}
}
}
//Average the files
f_name = "/1/0/";
list2 = getFileList(d+f_name);
```

```
f_name = "/2/0/";
list2 = getFileList(d+f_name);
for (i=0; i<221; i++) {
fullName = d + f_name+ list2[i];
fullName2 = d + "/2/0/"+ list2[i];
saveName = d + "/averaged/" + list2[i];
if (endsWith(fullName, ".tif")) {
open(fullName);
t = getTitle();
open(fullName2);
t2 = getTitle();
imageCalculator("Add create", t,t2);
selectWindow("Result of "+t);
dotIndex = lengthOf(saveName) - 4;
n = substring(saveName,0,dotIndex) + ".tif";
saveAs("Tiff", n);
close();
close();
close();
}
}
}
```

PROCESSING CODE

Runnable as a jython script

```
from ij import IJ
from ij import ImagePlus
from skeleton_analysis import AnalyzeSkeleton_
from Skeletonize3D_ import Skeletonize3D_
from skeleton_analysis import Point
from ij.gui import Wand
from ij.plugin.filter import Analyzer
from ij.process import PolygonFiller
from ij.measure import ResultsTable
import math
from os import listdir
from os.path import isfile, join


############
# This program is a python modification of the volume calculator program found at
#  https://github.com/fiji/fiji/commit/c220c0bfb61f1f786d9af5a510b588162cb751a0 .
#  This program performs volume calculation for an entire binary image without user
#  input.

########################
# Processing Constants
########################
minEdgeLength = 2.0;
AnalysisDirectory = "C:/ "
# Replace Analysis Directory with directory containing images in question
#####################################
# Process each .tif file in directory
#####################################
```

```
files = listdir(AnalysisDirectory) #listdir will give the file names

for f in files:
  if f.endswith(".tif"):
        fullName = join(AnalysisDirectory, f)

        print 'Opening: ' + fullName

        ######################
        # Get original image
        ######################
        print('Loading Image...')
        #original = IJ.getImage()  # Opens image selected currently open and selected
        original = IJ.openImage(fullName)
        imp = original.duplicate()
        print('Image Loaded')

        ##############
        # Skeletonize
        ##############
        # http://fiji.sc/javadoc/Skeletonize3D_/Skeletonize3D_.html
        print('Begining Skeletonization.....')
        skeletonize = Skeletonize3D_()
        skeletonize.setup("",imp)
        skeletonize.run(imp.getProcessor())
        print('Skeletonization Complete')

        ###################
        # Analyze Skeleton
        ###################
        # http://fiji.sc/javadoc/skeleton_analysis/AnalyzeSkeleton_.html
        #
https://github.com/fiji/AnalyzeSkeleton/blob/46eac2bbe8f4e2492324bc7457780980dd17cc3f/src/main/java/skeleton_a
nalysis/AnalyzeSkeleton_.java
        print('Begining Skeleton Analysis.....')
        analyze = AnalyzeSkeleton_()
        analyze.setup("", imp)
        pruneIndex =  AnalyzeSkeleton_.SHORTEST_BRANCH
        pruneEnds = False
        shortPath = False
        silent = True
        verbose = True
        asResults = analyze.run(pruneIndex, pruneEnds, shortPath, imp, silent, verbose)

        # Count number of total edges
        edgeCount = 0;
        for i in range(asResults.getNumOfTrees()):
                countEdges = asResults.graph[i].getEdges()
                for edge in countEdges:
                        if (edge.getLength() > minEdgeLength):
                                edgeCount += 1

        print('Skeleton Analysis Complete')



        ############################
        # Analyze Skeletonized data
        ############################
        # https://github.com/fiji/fiji/commit/c220c0bfb61f1f786d9af5a510b588162cb751a0
```

```
print('Begining Volume Calculation.....')
currentEdge=0

# New results table
extra_rt = ResultsTable()
extra_head = ['Branch length','V1 x', 'V1 y', 'V1 z','V2 x','V2 y', 'V2 z', 'Voxels (um^3)', 'Diameter (um)']

# Conversion factor for voxels to um cubed
volumeMultiplier = imp.getCalibration().pixelDepth *imp.getCalibration().pixelHeight *
imp.getCalibration().pixelWidth

# Calculate slice processors for each segment of the image
sliceProcessor = [None]*original.getNSlices()
for  i in range(original.getNSlices()):
        sliceProcessor[i] = original.getStack().getProcessor(i+1)


# Iterate through all treesand edges (aka sections of vasculature)
for i in range(asResults.getNumOfTrees()):
        listEdges = asResults.graph[i].getEdges()
        for edge in listEdges:
           # Only analyze edges with a length further than xxx um (currently not removing edges)
           if (edge.getLength() > minEdgeLength):
                totalVoxels = 0
                currentEdge = currentEdge + 1

                # Start of edge
                v1 = edge.getV1()
                p1 = v1.getPoints().get(0)
                # end of edge
                v2 = edge.getV2()
                p2 = v2.getPoints().get(0)

                # For all the points along this edge:
                # Move to the slice number z + 1 and run the Wand at the x, y
                # coordinates of the original (thresholded image).
                # NB: Adding 1 to slice number because this z is 0-based.
                        ####sliceProcessor = original.getStack().getProcessor(p1.z + 1)

                        # http://rsbweb.nih.gov/ij/developer/api/ij/gui/Wand.html
                        wand = Wand(sliceProcessor[p1.z])
                        wand.autoOutline(p1.x, p1.y)
                        # Calculate area within outline of vasculature
                        poly = PolygonFiller(wand.xpoints,wand.ypoints,wand.npoints)
                        mask = poly.getMask(original.width+1,original.width+1)
                        count = 0

                        xMin = min(wand.xpoints.tolist())
                        xMax = max(wand.xpoints.tolist())
                        maskArray = mask.getIntArray()
                        for y in range(xMin,xMax):
                                totalVoxels += (sum(maskArray[y])/255)

                        # Need to watch for a change in the value of the z coordinate
                        lastZpoint = (p1.z + 1)

                        for  point in edge.getSlabs():
                           # If the z position has not changed skip this point because
                           # the previous pixel is connected to this pixel.
                           if (point.z + 1) != lastZpoint:
```

```
                                        ####sliceProcessor = original.getStack().getProcessor(point.z + 1)
                                        wand = Wand(sliceProcessor[point.z])
                                        wand.autoOutline(point.x, point.y)
                                        # Calculate area within outline of vasculature
                                        poly = PolygonFiller(wand.xpoints,wand.ypoints,wand.npoints)
                                        mask = poly.getMask(original.width+1,original.width+1)
                                        count = 0
                                        maskArray = mask.getIntArray()
                                        xMin = min(wand.xpoints.tolist())
                                        xMax = max(wand.xpoints.tolist())
                                        for y in range(xMin,xMax):
                                                totalVoxels += (sum(maskArray[y])/255)
                                        #for x in range(mask.width):
                                        #   totalVoxels += (sum(maskArray[x])/255)
                                        lastZpoint = (point.z + 1)

                                    if lastZpoint != (p2.z + 1):
                                        # get the last point and count the surrounding pixels
                                        ####sliceProcessor = original.getStack().getProcessor(p2.z + 1)
                                        wand = Wand(sliceProcessor[point.z])
                                        wand.autoOutline(p2.x, p2.y)
                                        # Calculate area within outline of vasculature
                                        poly = PolygonFiller(wand.xpoints,wand.ypoints,wand.npoints)
                                        mask = poly.getMask(original.width+1,original.width+1)
                                        count = 0
                                        maskArray = mask.getIntArray()
                                        xMin = min(wand.xpoints.tolist())
                                        xMax = max(wand.xpoints.tolist())
                                        for y in range(xMin,xMax):
                                                totalVoxels += (sum(maskArray[y])/255)

                                # Calculate the diameter of the vasculature
                                diameter = 2*math.sqrt((totalVoxels*volumeMultiplier)/(edge.getLength()*math.pi))

                                # Add to output table
                                extra_rt.incrementCounter();
                                extra_rt.addValue(extra_head[0], edge.getLength())
extra_rt.addValue(extra_head[1], edge.getV1().getPoints().get(0).x * imp.getCalibration().pixelWidth)
extra_rt.addValue(extra_head[2], edge.getV1().getPoints().get(0).y * imp.getCalibration().pixelHeight)
extra_rt.addValue(extra_head[3], edge.getV1().getPoints().get(0).z * imp.getCalibration().pixelDepth)
extra_rt.addValue(extra_head[4], edge.getV2().getPoints().get(0).x * imp.getCalibration().pixelWidth)
extra_rt.addValue(extra_head[5], edge.getV2().getPoints().get(0).y * imp.getCalibration().pixelHeight)
extra_rt.addValue(extra_head[6], edge.getV2().getPoints().get(0).z * imp.getCalibration().pixelDepth)
                                        extra_rt.addValue(extra_head[7], totalVoxels*volumeMultiplier)
                                        extra_rt.addValue(extra_head[8], diameter)

                                        # Print out current table data and progress

 print 'Edge %d of %d, Length = %f, Diameter = %f' % (currentEdge,edgeCount,edge.getLength(),diameter)

        print('Volume Calculation Complete')
        #extra_rt.show("Branch information")

        ######################################
        # Save output file
        ######################################
        outName = 'Analysis' + f[:-3] + 'xls'
        fullOutName = join(AnalysisDirectory, outName)
        print 'Results saved in: ' + fullOutName
        extra_rt.saveAs(fullOutName)
```